Thermodynamic Properties of a Conformationally Constrained Intramolecular DNA Triple Helix†

Jens Völker,‡ Scott E. Osborne,§ Gary D. Glick,§ and Kenneth J. Breslauer*,‡

Department of Chemistry, Rutgers, The State University of New Jersey, P.O. Box 939, Piscataway, New Jersey 08855-0939, and Department of Chemistry, University of Michigan, Ann Arbor, Michigan 48109-1055

Received September 10, 1996; Revised Manuscript Received November 6, 1996⊗

ABSTRACT: We describe the thermodynamic properties of an intramolecular triple helix with two all-thymine linker loops in which the Hoogsteen strand is covalently crosslinked to the underlying Watson−Crick hairpin duplex by means of a disulfide bridge. We compare these properties to those of the corresponding intramolecular triplex without the disulfide crosslink. Optical and calorimetric measurements reveal that the uncrosslinked parent triplex melts in a biphasic manner above pH 6, with the initial triplex to duplex transition (Hoogsteen strand release) occurring at lower temperatures than subsequent melting of the hairpin helix. By contrast, crosslinking increases the thermal stability of the Hoogsteen transition such that the triplex and underlying hairpin duplex melt as a single transition under all conditions studied. Model independent thermodynamic data obtained by differential scanning calorimetry reveals the crosslink-induced increase in triplex thermal stability corresponds to a free energy stabilization of about 3 kcal/mol, with this stabilization being entirely entropic in origin. In other words, the crosslink is enthalpically neutral, but nevertheless, induces a triplex stabilization of 3 kcal/mol due to a reduction in the entropy change associated with triplex melting. In an effort to define the origin(s) of this entropic impact, we measured the pH and ionic strength dependence of the melting transitions. From a comparison of the melting transitions at different pH values and ionic strengths, we estimate that 0.4 more protons are associated with the crosslinked triplex state than with the uncrosslinked triplex, and 1.3 fewer counterions are released on melting the crosslinked triplex. We discuss how such crosslink-induced changes in proton binding and counterion release, in conjunction with potential changes in hydration and conformational freedom, could combine to give rise to the observed changes in entropy.

Custom-designed synthetic oligonucleotides frequently are used to model structural and thermodynamic properties of complex polymeric DNA molecules. Such oligomeric model systems can simplify the properties of more elaborate DNA molecules and hence provide a convenient means to gain insight into the characteristics of DNA molecules, particularly as they relate to their biological function(s) (van de Sande et al., 1988; Williamson, 1994; Seeman & Kallenbach, 1994; Plum et al., 1995; Pilch et al., 1995; Kool, 1996). Due to their short length, however, the physicochemical properties of oligonucleotides do not always compare favorably to those of larger, high molecular weight nucleic acids. For example, oligonucleotides have reduced thermal stabilities and greater end effects (Baldwin, 1971; Elson et al., 1970, Scheffler et al., 1970; Breslauer, 1986; Breslauer et al., 1986; SantaLucia et al., 1996; Record & Lohman, 1978; Ohlmsted et al., 1991; MacGregor, Jr., 1996) relative to their polymeric counterparts. Furthermore, unlike polymers, the denaturation of short oligonucleotides often is a bimolecular process in which the effects of helix initiation can dominate those of helix propagation (Craig et al., 1971; Pörschke, 1971, 1977; Pörschke & Eigen, 1971; Cantor & Schimmel, 1980b).

To overcome some of the limitations posed by the use of short oligonucleotides, model systems have been devised in which the termini are covalently crosslinked to each other. To this class of model compounds belong the DNA dumbbells first studied by Baldwin and co-workers (Baldwin, 1971; Erie et al., 1987, 1989; Wemmer & Benight, 1985; Benight et al., 1988; Doktycz et al., 1992; Amaratunga et al., 1992; Paner et al., 1992; Ashley & Kushlan, 1991; Germann et al., 1985), the DNA hairpins crosslinked in the stem region by a chemical crosslink (Glick, 1991; Cain et al., 1985; Wang et al., 1994, 1995), as well as the duplexes crosslinked by a chemical agent (Glick et al., 1992; Osborne et al., 1996a; Doktycz et al., 1993; Ferentz & Verdine, 1991; Ferentz et al., 1993).

Thermodynamic and structural studies of such constrained model systems have provided unique insights into the forces that stabilize DNA structures. For example, DNA dumbbells are useful systems for elucidating nearest neighbor parameters in duplex DNA (Docktycz et al., 1992) and for isolating the effect(s) of hairpin loop size on duplex stability (Amaratunga et al., 1992). In addition, studies on DNA dumbbells and chemically crosslinked duplexes have highlighted the importance of constrained denatured states for the stability of the complex (Osborne et al., 1996a; Erie et al., 1989). More recently, it has been shown that appropriately chosen dumbbell-like nucleic acid minicircles can combine with complementary DNA single strands to give rise to DNA triplexes with improved thermal stability (Prakash & Kool, 1991, 1992; Kool, 1991; Rubin & Kool, 1994; Rumney & Kool, 1993; Vo et al., 1995).

† This work was supported by National Institutes of Health Grants CA 47795 (K.J.B.), GM23509 (K.J.B.), GM 34469 (K.J.B.), and GM 53861 (G.D.G.).

* Author to whom all correspondence should be addressed. Tel: (908) 445-3956. Fax: 1 (908) 445-3409. E-mail: brslauer@rutchem.rutgers.edu.

‡ Rutgers.

§ University of Michigan.

⊗ Abstract published in *Advance ACS Abstracts,* January 1, 1997.

S0006-2960(96)02271-4 CCC: $14.00

The most common method to crosslink DNA duplexes is to link the DNA backbones by means of nucleotide hairpin loops (Erie, 1989; Docktycz, 1992) or some chemical variation thereof (Doktycz, 1993; Rumney & Kool, 1993). Due to topological constraints, such links can be incorporated only into structures made up of an even number of strands (duplexes, quadruplexes). In triple helical DNA structures, the uneven number of strands cause any hairpin−loop type crosslink to leave at least one strand unattached. To form conformationally constrained DNA triplexes, at least one (or possibly more) of the crosslink(s) has to be at the level of a nucleic acid base, which by necessity requires chemical modification of the relevant base. In this respect, the reversible disulfide crosslinking methodology developed by the Glick laboratory (Glick, 1991; Goodwin & Glick, 1993) allows for incorporation of such a conformational constraint into any higher-order nucleic acid structure. In this work, we characterize the thermal and thermodynamic consequences of incorporating a disulfide crosslink into the Hoogsteen strand of an oligonucleotide which previously has been shown to fold into an intramolecular DNA triple helix (Häner & Dervan, 1990). Such macroscopic characterizations of triplexes allows one to define the impact of synthetic alterations on the phase diagrams of these higher-order nucleic acid structures. On a practical level, such knowledge is essential for defining conditions under which altered triplex structures may be used to advantage in antisense technologies. On a fundamental level, such knowledge increases our understanding of the macroscopic impact of microscopic structural alterations, thereby enhancing our ability to more rationally design synthetic analogues with predictably altered properties.

The formation of conventional intramolecular triple helices in oligonucleotides containing an appropriate arrangement of purine and pyrimidine stretches connected by some loop region was first reported by Sklenar and Feigon (1990). These oligonucleotides fold into "hairpin with dangling tail" intermediates by conventional Watson−Crick base-pairing between a homopurine and its complementary homopyrimidine strand. The dangling tail binds to the major groove of the hairpin double helix via Hoogsteen base pairs (Hoogsteen, 1959) (if the tail consists of pyrimidines) or reverse Hoogsteen base pairs (if the tail consists mostly of purines), thereby resulting in an intramolecular triple helix (Völker et al., 1993; Häner & Dervan, 1990; Sklenar & Feigon, 1990; Radhakrishnan et al., 1991a,b, 1992a,b, 1993a,b; Radhakrishnan & Patel, 1993, 1994a−c; Durand et al., 1992). Such intramolecular triplexes have proven invaluable in elucidating many structural and thermodynamic aspects of pyrimidine·purine−pyrimidine[1] and purine·purine−pyrimidine triple helices. In particular, intramolecular triplexes have facilitated high-resolution NMR structural studies (Sklenar & Feigon, 1990; Macaya et al., 1991; Radhakrishnan et al., 1991a,b, 1992a,b, 1993a,b; Radhakrishnan & Patel, 1993, 1994a−c; Wang et al., 1992) and have simplified thermodynamic studies on DNA triplexes (Völker et al., 1993; Völker & Klump, 1994; Plum & Breslauer, 1995; Rentzeperis & Marky, 1995). These and other studies of intra- and intermolecular triple helices have resulted in considerable consensus concerning structural and thermodynamic aspects of triple helix formation, details of which may be found in several recent excellent reviews (Soyfer & Potaman, 1995; Plum et al., 1995; Radhakrishnan & Patel, 1994c; Thuong & Helene, 1993; Sun & Helene, 1993; Cheng & Pettitt, 1992).

In intramolecular triple helices, the three strands are linked in place by two oligonucleotide loop regions. Clearly only one additional tether is required in order to form a constrained system. In the system studied here, we have chosen to chemically crosslink the Hoogsteen strand to the underlying Watson−Crick hairpin via a disulfide bond, since we are mainly interested in the properties of the constrained higher-order nucleic acid structure. Note, however, that our methodology would also have enabled us to crosslink the free end of the Watson−Crick hairpin (Glick et al., 1992; Wang et al., 1994, 1995) or to crosslink both the hairpin and the Hoogsteen strand by two independent crosslinks.

The synthesis of the disulfide crosslinked triplex (Goodwin et al., 1994) and a preliminary structural characterization are described elsewhere (Osborne et al., 1996b). However, on the basis of structural studies alone no conclusions concerning the crosslink-induced changes in the thermal and thermodynamic stability of the molecule can be made. To more completely understand the consequences of introducing the disulfide crosslink into the intramolecular triplex, it is necessary to perform parallel thermodynamic studies on the crosslinked molecule and its uncrosslinked parent. Here we use spectroscopic and calorimetric techniques to define the thermal and thermodynamic consequences of the disulfide crosslink technology. Specifically, we use UV and CD spectroscopy to detect and identify the nature of the conformational states that the oligonucleotides assume and to monitor the temperature-induced transitions between these states. We also determine the effect of ionic strength and pH on these transitions and use this information to construct appropriate phase diagrams. Differential scanning calorimetric measurements at select conditions allows us to obtain model independent thermodynamic data for each transition. On the basis of these macroscopic data, we define the thermodynamic and extra thermodynamic consequences of incorporating a disulfide crosslink into an intramolecular triplex.

MATERIALS AND METHODS

Oligonucleotide Synthesis and Purification. Oligonucleotides ITS-TTA and ITS-xl-TTA shown in Chart 1 were synthesized and purified as previously described (Goodwin et al., 1994; Osborne et al., 1996b). After purification and desalting, the oligonucleotides were redissolved in pH 7.0 buffer A (see below). The molar extinction coefficient of the heat-denatured form of each oligonucleotide was determined by phosphate analysis (Snell & Snell, 1949) and is in reasonable agreement with the extinction coefficients obtained by summing the contributions of all neighbor bases (Cantor et al., 1970). In particular, the extinction coefficient of ITS-TTA was found to be $(2.87 \pm 0.01) \times 10^5$ mol^{-1} cm^{-1}, while that of ITS-xl-TTA was found to be $(2.74 \pm 0.01) \times 10^5$ mol^{-1} cm^{-1}.

Buffer Preparation. All studies were performed using a standard buffer (buffer A) consisting of 20 mM sodium acetate/acetic acid, 15 mM Na_2HPO_4/H_3PO_4, 1 mM EDTA,

[1] We shall adhere to the following notation throughout the text: the Hoogsteen strand precedes the Watson purine strand, which in turn precedes the Crick pyrimidine strand. Hoogsteen base-pairs are indicated by "·"; Watson−Crick base-pairs are indicated by "−".

Chart 1

ITS-TTA

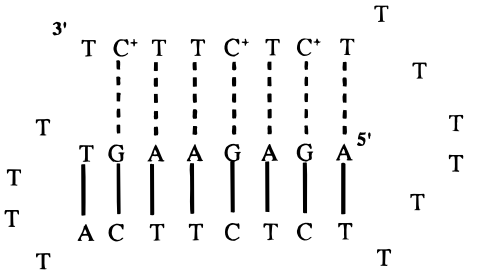

ITS-xl-TTA

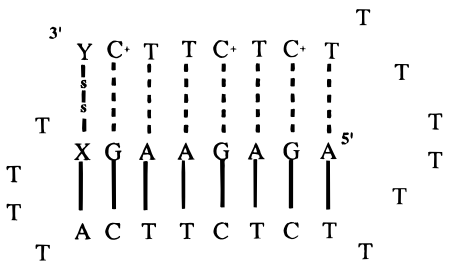

and NaCl in the appropriate ratios to give the desired pH and ionic strength. The target pH was obtained by mixing appropriate quantities of the base form of buffer A (20 mM sodium acetate, 15 mM Na_2HPO_4, 1 mM EDTA, 10 mM NaCl) with the acid form of buffer A (20 mM acetic acid, 15 mM H_3PO_4, 1 mM EDTA, 50 mM NaCl), while the desired ionic strength was obtained by mixing appropriate quantities of buffer A with buffer A containing 5 M NaCl (buffer A high salt).

UV Spectroscopy. Absorbance versus temperature profiles at 260 nm (UV-melting curves) were measured using a Perkin Elmer Lambda 4C UV/visible spectrophotometer interfaced via a National Instruments GPIB-SCSI controller to an Apple Maintosh computer. Samples were heated from 0.5 to 90 °C at a linear heating rate of 0.5 °C/min to ensure thermal equilibrium. Temperature/absorbance data points were collected in 40 s intervals (roughly 0.33 °C/data point), and the resulting temperature versus absorbance profiles were analyzed as previously described (Marky & Breslauer, 1987).

CD Spectroscopy. Circular dichroism measurements were performed using an Aviv DS60 (Aviv Associates, NJ) spectropolarimeter by automatically recording spectra between 360 and 200 nm in 5 °C intervals. For each spectrum, data points were recorded every 0.5 nm using a constant band width setting of 1.5 nm and an averaging time of 10 s per data point. Individual spectra were base line corrected to account for buffer/cuvette absorbances and smoothed using the algorithm provided by the manufacturer. To facilitate comparisons, molar ellipticities were calculated from the known oligonucleotide concentrations and the recorded spectra (Cantor & Schimmel, 1980).

Differential Scanning Calorimetry. Calorimetric melting profiles were obtained using either a Microcal MC2 differential scanning calorimeter (Microcal, Amherst, MA) or a DS93 (Johns Hopkins University, Baltimore, MD) differential scanning calorimeter. In each case the sample was repeatedly scanned from 0 to 100 °C at a constant heating rate of 1 °C/min, and the repeat scans were averaged. After subtraction of the appropriate buffer versus buffer base lines, the calorimetric enthalpy for each transition was derived by integrating the area of the excess apparent heat capacity curves (Marky & Breslauer, 1987). No evidence was found for a heat capacity change accompanying any of the traces (i.e., $\Delta C_p = 0$). The calorimetric entropy was calculated either by integrating the derived C_p/T melting profile or by applying the well known relationship $\Delta S_{cal} = \Delta H_{cal}/T_m$ (Marky & Breslauer, 1987). The results of both approaches were indistinguishable.

Analysis of the Phase Diagrams. The ionic strength dependence of each conformational transition was analyzed on the basis of the T_m versus log[Na^+] phase diagrams using the following relationship (Record et al., 1978):

$$d(1/T_m)/d(\log[a_L]) = (R \ln 10/\Delta H_{cal})\Delta n_L \qquad (1)$$

In this case [a_L] corresponds to the mean molal sodium chloride activity [a_{NaCl}] and $\Delta n_L = \Delta n_{Na^+} = n_{Na^+(coil)} - n_{Na^+(helix)}$ corresponds to the total amount of Na^+ counterions released or taken up on melting. (Strictly speaking, Δn_L corresponds to the total release of anions and cations. However, due to the large negative charge density of the DNA, anion binding/release can to a first approximation be considered insignificant.) The derivative $d(1/T_m)/d(\log[a_L])$ represents the slope of the $1/T_m$ vs log[a_{NaCl}] curve, R is the universal gas constant, and ΔH_{cal} corresponds to the calorimetric enthalpy for the transition. The mean molal sodium chloride activity [a_{NaCl}] for each ionic strength was calculated from the known sodium ion concentration [Na^+] and assuming only chloride counterions, as previously described (Plum & Breslauer, 1995). Clearly neglecting contributions from all other buffer components to the mean molal NaCl activity will give rise to errors in activity coefficients. However, we judge these errors to be small in comparison with the overall uncertainty in determining the solution activity. Briefly, the molal Na^+ concentration (m_{Na^+}) was calculated from the known molar Na^+ concentration (M_{Na^+}) and the known density of sodium chloride solutions at 25 °C (Weast, 1982). The mean electrolyte activity then was calculated using the relationship $a_{NaCl} = m_{Na^+}\gamma_{NaCl}$, where γ_{NaCl}, the mean molal activity coefficient for NaCl at 25 °C, was taken from Robinson and Stokes (1959) as described by Plum and Breslauer (1995). Since it was previously found that the temperature coefficients of γ_{NaCl} are small (Plum & Breslauer, 1985), no corrections for temperature effects of a_{NaCl} were made.

The pH dependence of each conformational transition was analyzed from the T_m versus pH phase diagrams according to the following equation (Plum & Breslauer, 1995; Record et al., 1976; Ptitsyn & Birshtein, 1969; Pfeil & Privalov, 1976):

$$d(1/T_m)/d(pH) = -(R \ln 10/\Delta H_{cal})\Delta k \qquad (2)$$

where $d(1/T_m)/d(pH)$ represents the slope of the $1/T_m$ vs pH curve, $\Delta k = k_{coil} - k_{helix}$ corresponds to the amount of protons released or taken up during the transition, and all other variables are as described. Since by definition the pH corresponds to the negative logarithm of the hydrogen ion activity ($-\log_{10}[a_{H^+}]$), the analogy of this equation to eq 1 used to analyze the ionic strength dependence of the phase transitions should be readily apparent.

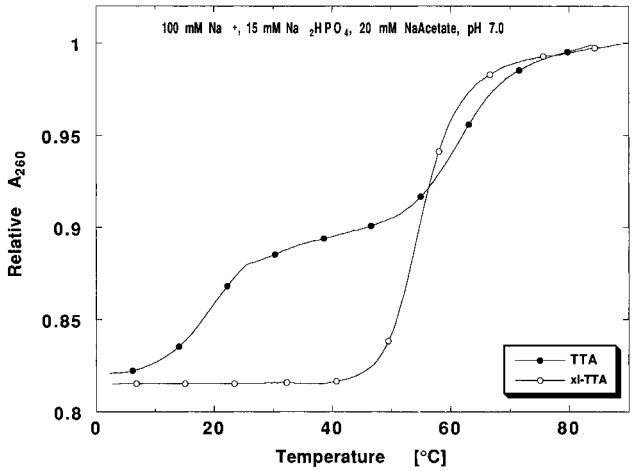

FIGURE 1: UV absorbance at 260 nm as a function of temperature for the uncrosslinked oligonucleotide ITS-TTA (●) and the crosslinked oligonucleotide ITS-xl-TTA (○) in 100 mM Na^+ buffer, pH 7.0.

RESULTS AND DISCUSSION

Temperature-Dependent UV Absorbance Studies at pH 7.0

Crosslinking Increases Triplex Thermal Stability While Altering the Triplex Melting Pathway. Figure 1 compares the pH 7.0 UV melting profiles at 100 mM Na^+ for the parent uncrosslinked triplex (●) and for the crosslinked triplex constrained by one disulfide bridge (○). Note that the uncrosslinked triplex melts in two well-resolved transitions with T_m values of 18.8 ± 1 and 61.4 ± 1 °C, respectively, consistent with the melting behavior of other such triplexes (Völker et al., 1993; Völker & Klump, 1994; Plum & Breslauer, 1995). By contrast, the crosslinked triplex melts in an apparent monophasic manner, with a T_m of 54.7 ± 1 °C. Further, the total hyperchromic change associated with the two-step melting of the uncrosslinked triplex corresponds closely to the total hyperchromic change associated with the one-step melting of the crosslinked triplex. This correspondence suggests a similar degree of net base unstacking for both overall denaturation processes.

One interpretation consistent with the above observations is that crosslinking induces an increase in the thermal stability of the initial triplex such that the triplex and underlying duplex melt as a single transition, rather than as two thermally resolved melting events, as occurs with the uncrosslinked triplex. In other words, crosslinking changes the path by which the initial triple helical state denatures to a less ordered, final "coiled" state, an observation which is consistent with NMR studies on these same molecules (Osborne et al., 1996b). In the section that follows, we describe how we confirm this interpretation by using CD measurements to define the different interconverting states.

Temperature-Dependent CD Studies at pH 7.0

Crosslinking Precludes Formation of an Intermediate Duplex State During Triplex Melting. Panels A and B of Figure 2 show the pH 7.0 CD spectra at 100 mM Na^+ for the parent, uncrosslinked triple helix over a range of temperatures (panel A, 0−40 °C, and panel B, 35−90 °C). Panel C shows the corresponding spectra from 0 to 90 °C for the disulfide-crosslinked triplex. Note that at low

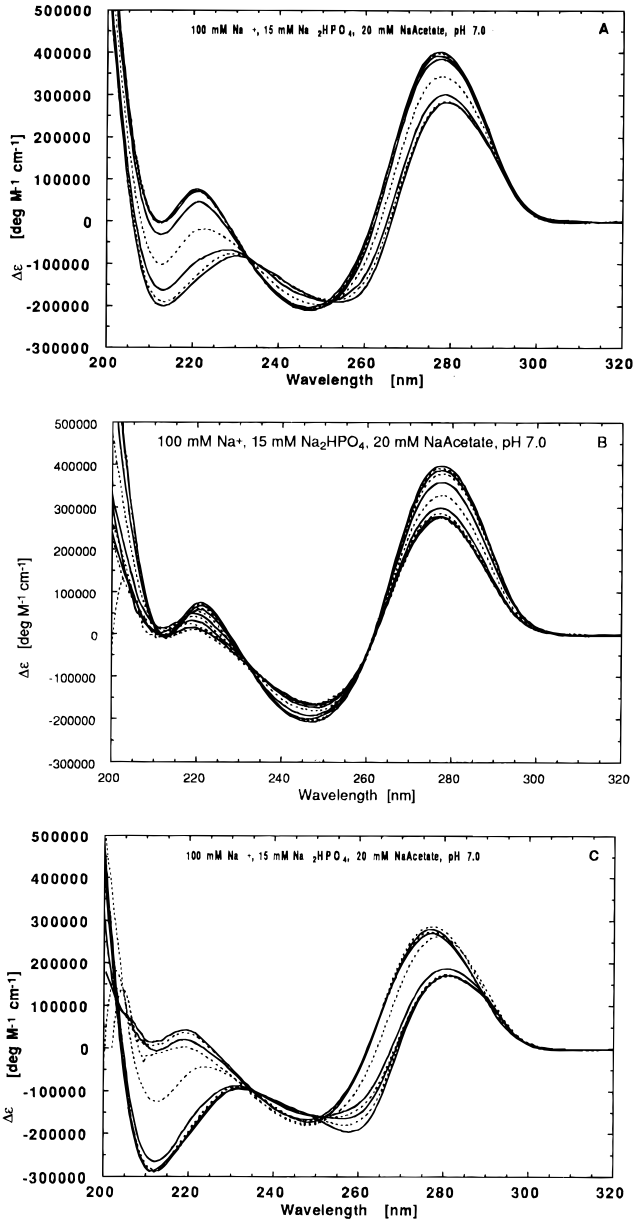

FIGURE 2: CD spectra as a function of temperature for the uncrosslinked oligonucleotide ITS-TTA (panels A and B) and the crosslinked oligonucleotide ITS-xl-TTA (panel C) in a 100 mM Na^+ buffer, pH 7.0. To better illustrate the two sequential transitions observed for ITS-TTA, panel A shows the CD spectra in the temperature range 0−40 °C, while panel B shows the CD spectra in the temperature range 35−90 °C. Panel C illustrates the single cooperative transition observed for ITS-xl-TTA in the temperature range 0 to 90 °C.

temperatures both the uncrosslinked and crosslinked structures exhibit negative bands at 213−214 nm, a property characteristic of triple helices (Gray et al., 1995; Callahan et al., 1991; Steely et al., 1986; Plum & Breslauer, 1995). In other words, at low temperature both the uncrosslinked and crosslinked structures exist in solution as triplexes. With increasing temperature, the uncrosslinked structure undergoes two sequential transformations, with each transition reflected by the CD spectral changes shown in panel A (0−40 °C) and panel B (35−90 °C). Note that in panel A we observe initial loss of the 213−214 nm negative band, accompanied by an increase in intensity and slight blue-shift of the 280 nm positive band, changes characteristic of duplex formation from a triplex state. At higher temperatures, as shown in

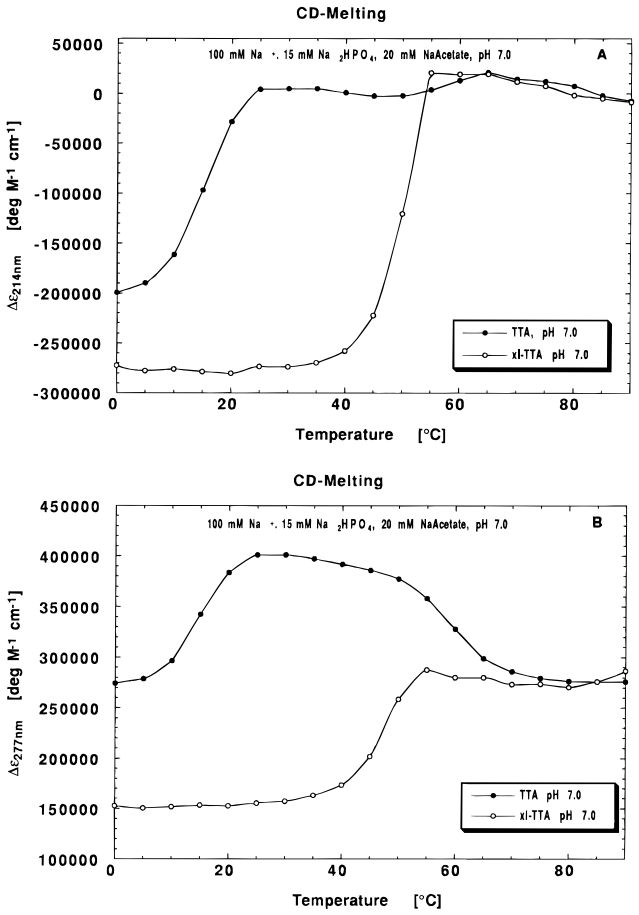

FIGURE 3: CD melting curves for ITS-TTA (●) and ITS-xl-TTA (○) monitored at 214 nm (A) and 277 nm (B).

panel B, we observe a spectral shape reflective of subsequent formation of a single-stranded structure, primarily characterized by a decrease in positive ellipticity at 277 nm. In contrast to this behavior, for the crosslinked structure, as shown in panel C, increasing the temperature causes the CD spectra to go directly from shapes characteristic of a triplex state (with a negative band at 213−214 nm) to spectra consistent with a final single-stranded state. In other words, in contrast to the sequential triplex-to-duplex and duplex-to-single-strand melting of the uncrosslinked triplex, crosslinking causes the triplex state to melt directly to the final single-stranded state, with no apparent intermediary of a duplex state.

These characteristic alterations in the CD spectra are best followed by monitoring the temperature induced change in the CD signal at a single wavelength, preferably one which corresponds to the maximum change in ellipticity. Figure 3 shows such CD melting curves at 214 nm (panel A) and at 277 nm (panel B) derived from the temperature-induced changes in the CD spectra described above. Note that for the uncrosslinked oligonucleotide (●), the initial triplex-to-duplex melting event at low temperatures is clearly revealed at both 214 and 277 nm, while the subsequent higher-temperature denaturation of the duplex state shows up most clearly at 277 nm, as expected for duplex melting. In contrast to this melting behavior, for the uncrosslinked triplex only one transition is detected at both wavelengths, with this transition corresponding to the direct transformation of the initial triple helical state to its final "single-stranded" state. In these CD melting curves, no evidence for an intermediate duplex state exists at any temperature. Panels A and B of Figure 3 also reveal that the intensity of the CD signals of the high-temperature denatured state of both oligonucleotides agrees to within the noise of the measurement, while significant differences exist in the intensity of the CD signals of the native states. These observations suggest that crosslinking may result in some small local perturbations in the structure of the native triplex state, in agreement with the NMR results obtained for this and a related disulfide-crosslinked triplex (Osborne et al, 1996b). The similarity of the CD signals of the denatured states may reflect a similar degree of base unstacking in both molecules at the elevated temperatures, although such a conclusion may well exceed the information content of the CD measurement. To obtain more quantitative evidence for the assertions noted above, we also subjected our CD spectra to a SVD analysis to extract the principle spectral components and to assess how these components change with temperature. The conclusions derived from this analysis (not shown) are fully consistent with those derived from inspection of the experimental CD spectra.

In the aggregate, we can summarize the CD data as follows. The melting of the unconstrained structure involves conversion of an initial triplex state to an intermediate duplex state, followed by melting of this duplex to form a final single-stranded state. This sequential melting behavior is in agreement with previous studies of other such intramolecular triplexes (Plum & Breslauer, 1995; Völker et al., 1993; Völker & Klump, 1994; Durand et al., 1992). By contrast, the melting of the constrained structure involves the conversion of an initial triplex state directly to a final single-stranded state, without significant population of an intermediate duplex form. These two transition pathways can be represented schematically by the cartoons shown in panels A and B of Figure 4. Note that the melting pathway of the uncrosslinked triplex (panel A) initially produces a hairpin duplex with a dangling 3′ single strand prior to melting to an extended single strand. By contrast, based on our optical measurements, we propose that the crosslinked triplex melts directly to a constrained "lariat-like" final "single-stranded" state, with a hypothetical intermediate constrained hairpin duplex shown in brackets to emphasize that we detect no evidence for its existence. Support for such a one-step transition is provided in a later section in which a comparison of our calorimeric and van't Hoff transition enthalpies reveal this transition to be a two-state process. However, before presenting and discussing our calorimetric measurements, we first describe in the sections which follow pH dependent melting studies which permit us to construct phase diagrams for both the unconstrained and constrained triplex structures.

pH Dependence of Triplex Melting

Biphasic Melting of the Uncrosslinked Triplex Becomes Monophasic at pH Values Below 7.0, While the Melting of the Crosslinked Triplex Remains Monophasic over the Entire pH Range Studied. Panels A and B of Figure 5 show the influence of pH on the melting behavior of the uncrosslinked and crosslinked triplexes, respectively. For the uncrosslinked triplex (panel A), note that the pH 7.0 biphasic melting behavior described above at 100 mM Na^+ disappears at pH values below pH 6.0. This observation is consistent with a pH-induced increase in triplex thermal stability such that

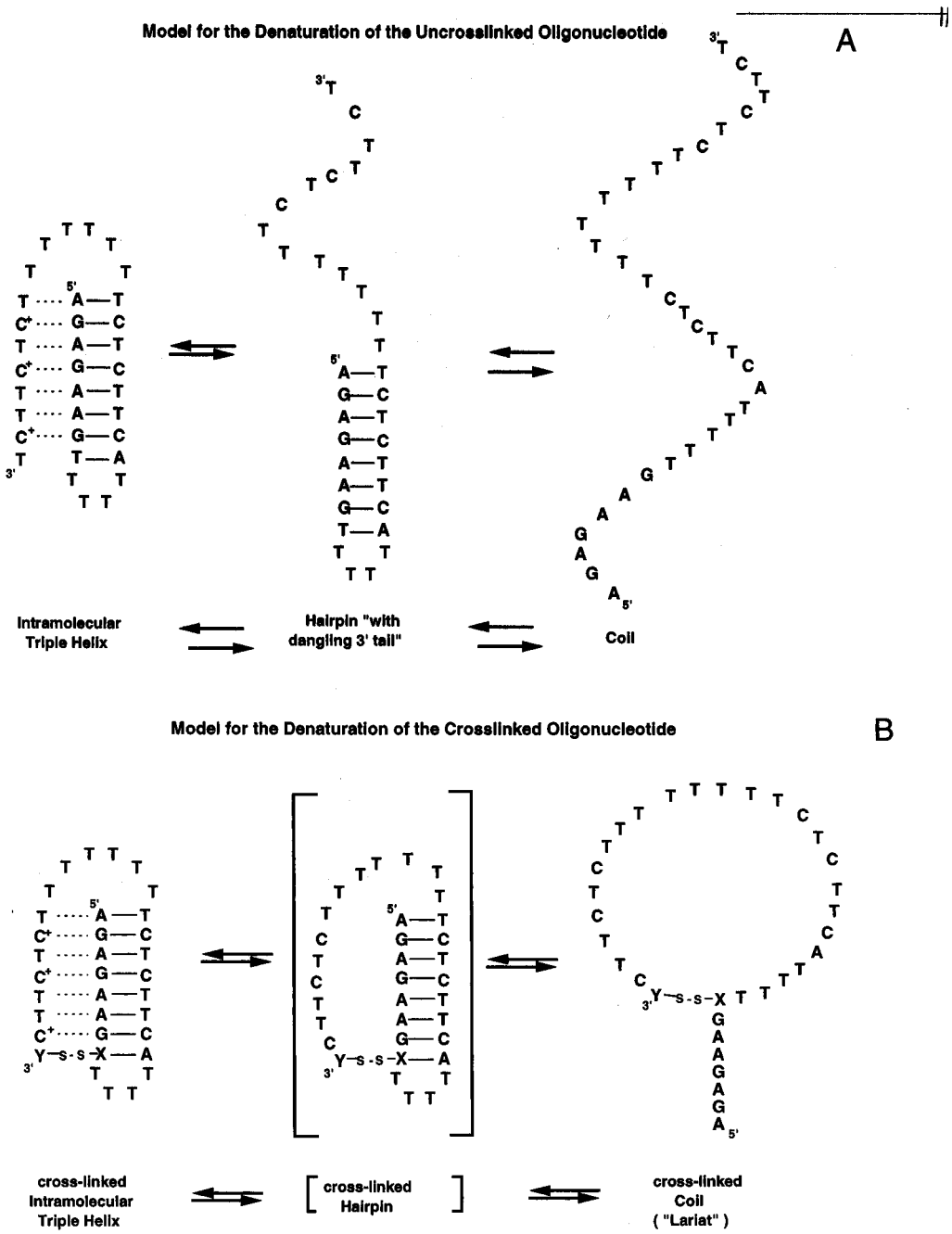

FIGURE 4: Schematic representation of the temperature-induced unfolding pathway of the uncrosslinked (panel A) and and crosslinked triplex (panel B). In panel B, the hypothetical crosslinked hairpin intermediate state is shown in brackets to indicate that it is not detected experimentally.

triplex melting occurs at a temperature where the intermediate duplex state no longer is thermally stable, thereby resulting in the transformation of the triplex directly into the single-stranded state at pH values below pH 6.0. By contrast, as shown in panel B, the melting profile of the crosslinked structure remains monophasic over the entire pH range studied, although the T_m increases with decreasing pH. These observations are consistent with the crosslinked structure melting directly from the triple helix to the single-stranded state over the entire pH range studied. The increase in triplex thermal stability observed as the pH is lowered is as expected and can be attributed to a pH-induced shift in the apparent equilibrium from the unprotonated/unbound Hoogsteen cytosines to the protonated/bound Hoogsteen cytosines.

Phase Diagrams

We have combined the information obtained from the temperature- and pH dependent UV and CD spectra discussed above to construct the phase diagrams shown in panels A and B of Figure 6 for the uncrosslinked and crosslinked triplexes, respectively, at 100 mM Na^+. These figures map which states interconvert under a given set of pH and temperature values. The interconverting states are noted by the Roman numerals (**III** = triplex, **II** = duplex, **I** = "single-strand"), while the arrows designate the transitions between these states. Inspection of the pH−*T* phase diagram for the uncrosslinked structure (panel A) reveals that it contains domains which correspond to three different classes of transitions: the triplex (III)-to-single-strand (I), the triplex

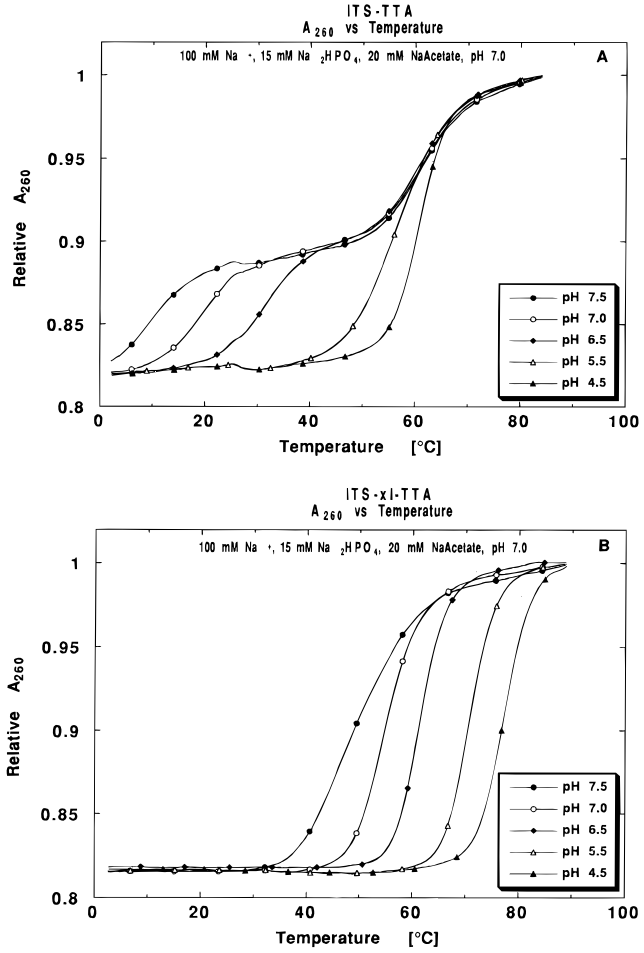

FIGURE 5: Absorbance versus temperature profiles at different pH values. Panel A shows the characteristic UV melting profiles for the uncrosslinked triplex ITS-TTA. The biphasic transition at high pH becomes monophasic at pH values below pH 6.0. Panel B shows the characteristic UV melting profiles for the crosslinked triplex ITS-xl-TTA. The transition remains monophasic over the entire pH range.

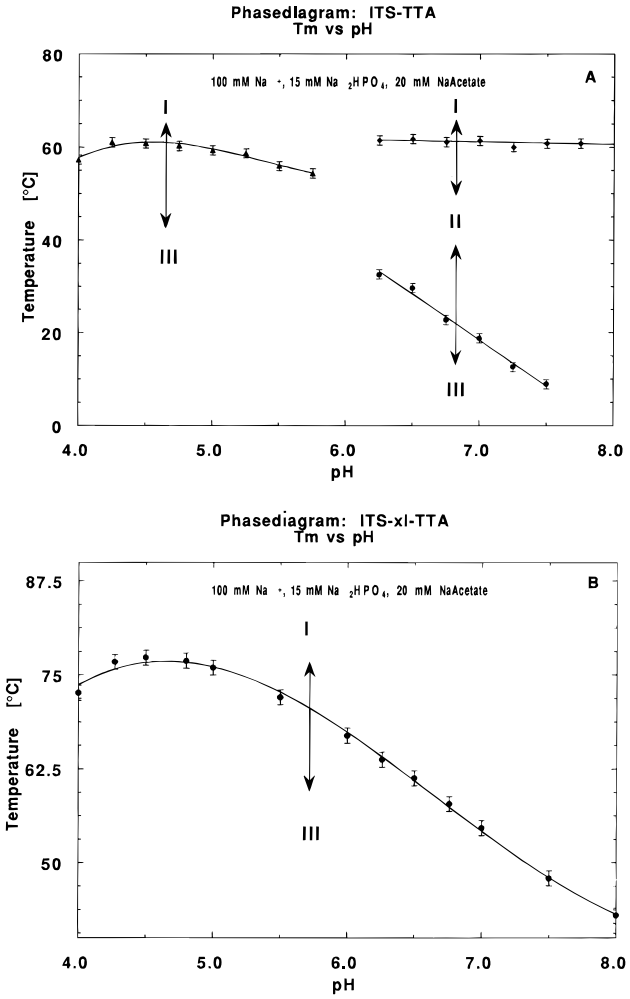

FIGURE 6: pH phase diagram for the uncrosslinked triplex ITS-TTA (panel A) and the crosslinked triplex ITS-xl-TTA (panel B) The roman numerals indicate the number of "strands" associated with each state: **III** corresponds to the triple helix, **II** corresponds to the duplex, and **I** corresponds to the "single strand". The arrows indicate the temperature-induced conformational transitions between these states.

(III)-to-duplex (II), and the duplex (II)-to-single-strand (I) transitions. By contrast the pH−T phase diagram of the crosslinked structure (panel B) contains just a single domain, reflective of only the triplex (III)-to-single-strand (I) transition. These two phase diagrams dramatically illustrate the impact of crosslinking on the pH and temperature-dependent states accessible to the molecule. In a later section, we will describe the impact of salt concentration on these transitions.

Triplex Melting Thermodynamics

Crosslinking Results in No Net Change in Enthalpy for the Overall Triplex to Coil Transition. Figure 7 shows the calorimetric melting profiles at pH 7.0 for the uncrosslinked (panel A) and crosslinked (panel B) triplexes. The observed biphasic (panel A) and monophasic (panel B) melting behaviors are consistent with the temperature-dependent UV and CD results described above. Furthermore, despite significant concentration differences, the T_m values derived from these calorimetric curves are consistent with those extracted from the corresponding optical melting profiles (see Table 1), as one would expect for monomolecular transitions. These calorimetric measurements also allow us to obtain complete thermodynamic profiles for each melting event. As described in the methods section, integration of the area under each heat capacity curve yields the transition enthalpy data, ΔH_{cal}, which are listed in the third data column of Table 1. Note that for the uncrosslinked structure, the thermally-induced triplex to duplex conversion exhibits a transition enthalpy of 33.9 kcal/(mol of triplex), while the subsequent duplex-to-single-strand transition exhibits a transition enthalpy of 53.9 kcal/(mol of duplex). The latter value for duplex melting is in excellent agreement with the enthalpy value of 50.2 kcal/(mol of duplex) predicted from nearest neighbor data (Breslauer et al., 1986). This agreement suggests that, at the duplex melting temperature, the single-stranded 3′ dangling end shown schematically in panel A of Figure 4 contributes relatively little to the enthalpy of duplex melting. The value of 33.9 kcal/(mol of triplex) that we measure for the triplex-to-duplex transition falls within the range of published values (Plum et al., 1990, 1995; Plum & Breslauer, 1995; Soyfer & Potoman, 1995) for Hoogsteen transitions, although, as expected, it is considerably less than the enthalpy of 53.9 kcal/(mol of duplex) associated with the duplex-to-single-strand transition. Using "Hess' Law", the sum of these two transition enthalpies yields a predicted value of 87.8 kcal/mol for the enthalpy associated with the overall conversion of the uncrosslinked triplex to the single-

Table 1: Comparison of Calorimetric and van't Hoff Thermodynamic Data for the Melting Transitions of the Uncrosslinked and Crosslinked Triplexes

	T_m[a] (cal)	T_m[a] (UV)	ΔH_{cal}[b]	ΔH_{vH} (cal)	ΔH_{vH}[c] (UV)	ΔS_{cal}[b]	ΔS_{vH} (cal)	ΔS_{vH}[c] (UV)	ΔG_{cal}[a]	ΔG_{vH} (cal)	ΔG_{vH}[c] (UV)
pH 7.0	[°C]	[°C]	[kcal/M]	[kcal/M]	[kcal/M]	[eu]	[eu]	[eu]	[kcal/M]	[kcal/M]	[kcal/M]
3 ↔ 2 TTA	20.0	18.8	33.9	48.6	51.0	115.7	165.8	174.7	-0.59	-0.82	-1.08
2 ↔ 1 TTA	61.1	61.4	53.9	61.2	61.9	160.8	183.1	185.1	5.97	6.62	6.77
3 ↔ 1 calcd TTA	44.4	40.7	87.8	109.8	112.9	276.5	348.9	359.8	5.38	5.79	5.64
3 ↔ 1 xl-TTA	55.4	54.7	87.9	87.5	77.5	267.2	266.4	236.4	8.25	8.09	7.03
pH 5.0											
3 ↔ 1 TTA	61.3	59.3	94.7[d]	N/A	78.7	283.2	N/A	236.8	10.28	N/A	8.11
3 ↔ 1 xl-TTA	77.1	75.9	98.1	116.9	108.7	280.1	333.8	311.4	14.60	17.39	15.87

[a] The T_m values have an estimated uncertainty of ±1.0 °C. [b] Except for the Hoogsteen transition of TTA (3 ↔ 2) the calorimetric values have an uncertainty of the order of 5%. The uncertainty for the 3 ↔ 2 transition of TTA is estimated to be of the order of 10%, due to the ill-defined lower base line. [c] The estimated uncertainty of the van't Hoff values is of the order of 5%. [d] Extrapolated value: reaction not reversible, i.e., area under the curve becoming progressively smaller. ΔH_{cal} value calculated by linear extrapolation to first scan. No degradation detected by HPLC.

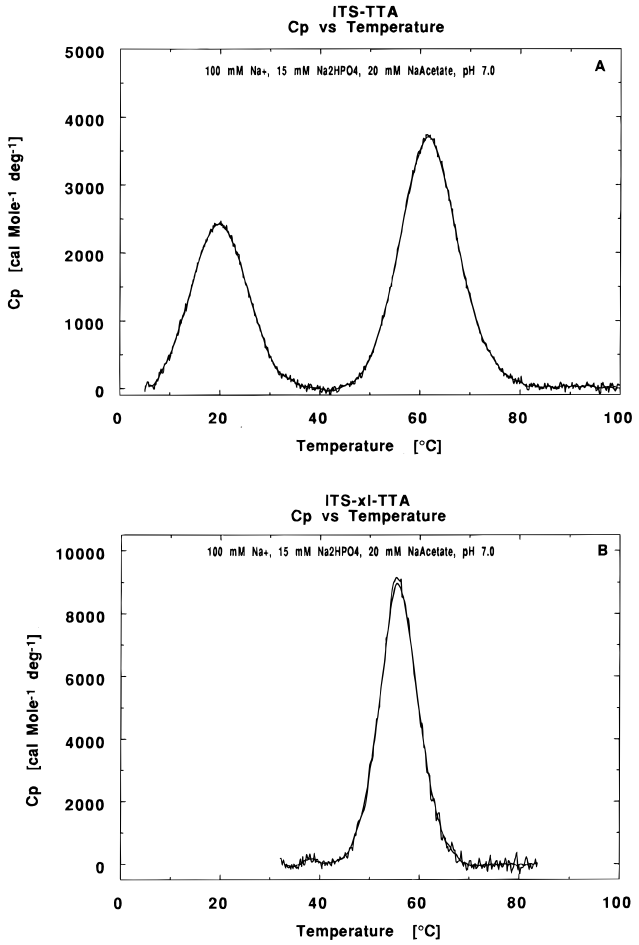

FIGURE 7: Apparent excess heat capacity vs temperature curve measured by differential scanning calorimetry for the uncrosslinked triplex (panel A) and the crosslinked triplex (panel B).

stranded state at pH 7.0. This calculated enthalpy value can be compared to the enthalpy we have measured for the corresponding triplex to "single-strand" transition of the crosslinked structure in order to assess the overall enthalpic impact of crosslinking. The latter enthalpy was obtained by integration of the area under the heat capacity curve shown in panel B of Figure 7. This integration yields 87.9 kcal/mol for the enthalpy of melting of the crosslinked structure, a value which is essentially identical with the enthalpy of 87.8 kcal/mol associated with the overall melting of the uncrosslinked structure. This agreement suggests that the significant impact of crosslinking on triplex thermal stability that we have noted ($\Delta T_m = 36$ °C) does not derive from net enthalpic differences between the initial triplex states and their corresponding final single-stranded states but rather from the entropic consequences of crosslinking.

The identity between the enthalpies associated with the triplex-to-single-stranded transitions of the crosslinked and uncrosslinked structures noted above may result from fortuitous compensation of crosslink-induced enthalpic effects in both the initial and final states. Alternatively, the enthalpic identity could reflect crosslinking in both the initial and final states being enthalpically neutral events. Although our data cannot differentiate between these two extreme possibilities, as described below we can use the calorimetric data to derive complete thermodynamic profiles for the uncrosslinked and crosslinked structures.

Crosslinking Results in an Increase in Triplex Stability Due to a Net Decrease in the Entropic Driving Force Favoring Triplex Melting. The intramolecular design of the triplex systems studied here causes all transitions to be monomolecular. Consequently, we can calculate entropy changes using the directly measured ΔH and T_m values and the relationship $\Delta S = \Delta H/T_m$. This approach yields the entropy values, ΔS_{cal}, listed in the sixth data column of Table 1, that are identical to those we obtain by integration of the derived C_p/T versus T heat capacity curve (Marky & Breslauer, 1987; Breslauer, 1994, 1995), as one would expect for a monomolecular transition. As with the enthalpy data, the entropy changes associated with the two pH 7.0 transitions for the uncrosslinked structure can be summed to obtain an overall entropy change of +276.5 eu for the triplex-to-single-strand transition of this molecule. This entropy change corresponds to a $T\Delta S$ contribution of 82.4 kcal/mol at 25 °C to the free energy of melting the uncrosslinked triplex. These numbers should be compared to the ΔS value of 267.2 eu for the triplex-to-"single-strand" transition of the crosslinked molecule, which corresponds to a $T\Delta S$ contribution of 79.6 kcal/mol at 25 °C to the free energy of melting. The $T\Delta\Delta S$ difference of 2.8 kcal (82.4−79.6) reflects the crosslinking-induced reduction in the entropic driving force favoring triplex melting to the coil state. This entropic impact of crosslinking on the triplex to coil transition is fully expressed in the free energy term since our calorimetric data reveal that crosslinking is enthalpically neutral. Thus, as reflected by the ΔG°_{cal} values listed in the ninth data column of Table 1, crosslinking results in a 2.8 kcal increase in triplex stability relative to the coil state [8.25 vs 5.38 (−0.59 + 5.97) kcal/mol]. In the section that follows, we discuss possible microscopic origins of these macroscopic data.

Potential Origins of the Entropic Consequences of Crosslinking. Exclusively on the basis of configurational considerations, crosslinking is expected to entropically destabilize both the native and the denatured states relative to their uncrosslinked counterparts. One might also expect the magnitude of the crosslink-induced change in configurational entropy of the native state to be significantly smaller than the magnitude of the crosslink-induced change in configurational entropy of the denatured state, since the native triplex already is configurationally constrained by Hoogsteen base pair formation. Thus, on the basis of configurational arguments alone, one might expect the crosslinked triplex to exhibit a net entropic stabilization (i.e., exhibit a lower entropy of denaturation) due to the more constrained lariat-like final state. Indeed, our experimental entropy data are consistent with this expectation, with the uncrosslinked triplex-to-single-strand melting event being entropically driven by 9.3 eu more (276.5−267.2 eu) than the corresponding melting event for the crosslinked triplex, although we recognize that this difference is close to the uncertainty in the data. Interestingly, however, the experimentally observed entropy change of 9.3 eu due to crosslinking is modeled extremely well by the calculated entropy changes of 11.3 or 12.4 eu for constraining the denatured state based on the probability of ring closure of an appropriate random chain (27 statistical segments of 3.4 or 4.1 Å in length) using the formalism of Jacobson and Stockmeyer (1950). On the basis of this apparent consistency, one might argue that the impact of the crosslink is due mainly to constraining the denatured state of the triple helix, with little or no contributions resulting from constraining the native state. However, one must keep in mind that the overall entropy change we calculate from the calorimetric data reflects contributions from differential solvation and counterion release, as well as from configurational effects. In fact, as discussed below, crosslinking induces significant differences in the degree of counterion/proton binding/release for the conformationally constrained triplex. It also is reasonable to expect some differences in the degree of solvation. Currently, it is not possible to estimate the entropic impact of such differential solvation/counterion (de)-binding phenomena. Consequently, a full account of the various component contributions to the total observed entropy change cannot be given at this time. Nevertheless, independent of our ability to resolve these component contributions, our data reveal the net entropic impact of crosslinking to reduce by about 3 kcal the free energy driving force favoring the triplex-to-coil melting process. In other words, crosslinking results in entropic stabilization of the triplex state by about 3 kcal.

Extra Thermodynamic Consequences of Crosslinking

van't Hoff Versus Calorimetric Melting Enthalpies and the Nature of the Transitions. We have analyzed the shapes of the DSC melting profiles at pH 7.0 for the uncrosslinked and crosslinked triplexes to obtain the model-dependent van't Hoff transition enthalpies listed in the fourth data column of Table 1. Note the good agreement between the calorimetric and van't Hoff values for the melting of the crosslinked structure. This agreement demonstrates that, under these conditions, the triplex to "single-strand" transition of the crosslinked structure occurs in an approximately two-state manner, with no significant population of intermediate states. Further inspection of the data in Table 1 reveals somewhat different behavior for the uncrosslinked structure. For the triplex-to-duplex plus single strand transition, we find the van't Hoff enthalpy to be higher than the corresponding calorimetric value. This curious disparity previously has been noted by us and others for such third-strand expulsion and Hoogsteen transitions and to date remains unexplained (Plum et al., 1990, 1995; Plum & Breslauer, 1995; Völker et al., 1993; Wilson et al., 1994). By contrast, the calorimetric and van't Hoff enthalpies for the subsequent duplex-to-single-strand transition of the uncrosslinked structure are similar, within the experimental uncertainty. This qualitative agreement suggests a near-two-state event for the duplex-to-single-strand transition, a result consistent with previous observations on other short duplexes (Breslauer, 1986; Breslauer et al., 1986).

Impact of Crosslinking on Melting Induced Changes in Counterion Condensation and Proton Binding. On the basis of a formalism outlined by Record et al. (1978), it is possible to estimate from salt and pH dependent melting behavior the change in the degree of counterion condensation (Manning, 1978) and proton binding (Record et al., 1976) associated with the denaturation of a poly/oligoelectrolyte. By applying this formalism to the thermally-induced transitions of the uncrosslinked and crosslinked triplexes, we have calculated the degree of counterion (Δn) and proton release (Δk) associated with each of the relevant transitions (see Methods). These data are listed in Table 2. For the biphasic melting of the uncrosslinked triplex, we calculate the overall counterion/proton release for the hypothetical triplex to single-stranded state in a manner analogous to our calculations of the thermodynamic functions of state. However, for reasons discussed in the paragraph that follows, it is not clear if such a simple additive approach is justified for estimating the overall release of counterions/protons for a "hypothetical" one-step triplex-to-coil transition in a pH range where the transition actually is biphasic.

In principle, the calculated number of counterions/protons released in going from a native to a denatured state should be independent of the transition path. This assertion is true since the change in the melting temperature with counterion concentration or pH can be considered to result from changes in the chemical potential (μ) of the electrolyte/proton concentration in solution. However, since the proton counterions interact with the oligonucleotides by site binding in the interior of the triple helix [which is outside the scope of the counterion condensation theory (Manning 1987)], while the Na^+ counterions are condensed onto the exterior, mutual influences ("cross-talk") between these two classes of "counterions" may modulate their individual interactions in unknown ways. Indeed, it previously has been observed (Völker & Klump, 1994) that $dT_m/d \log[Na^+]$ values for protonated DNA triple helices depend in nontrivial ways on the number and relative position(s) of potential protonation sites in the DNA structure. Furthermore, counterion condensation theory only should be applied to polymers with a ratio of polyion length to polyion diameter close to infinity (Manning, 1987; Olmstead et al., 1989, 1991; Record & Lohman, 1978). Clearly this condition is not met by the small oligoions studied here. With an awareness of these concerns, yet a desire to compare our results with other similar analyses of oligoions in the literature, we have calculated the counterion and proton release for the pH 7.0

Table 2: Dependence of the Triplex and Duplex Thermal Stabilities on [Na^+] and pH, and the Derived Degrees of Sodium Ion and Proton Release/Uptake upon Thermally-Induced Unfolding of the Crosslinked and Uncrosslinked Triplexes

	pH 7.5		pH 7.0		pH 6.5		pH 5.5		pH 4.5		100m	
	dT_m/d log[Na^+]	Δn	dT_m/d log [Na^+]	Δn	dT_m/d log[Na^+]	Δn	dT_m/d log[Na^+]	Δn	dT_m/d log[Na^+]	Δn	dT_m/d pH	Δk
3 ↔ 2 TTA	–		6.52 ± 0.4	0.621 ±0.07	6.38 ± 0.4	0.562 ± 0.07	–		–		−19.85 ± 0.9	1.71 ± 0.17
2 ↔ 1 TTA	14.25 ± 0.5	1.704 ± 0.18	13.69 ± 0.6	1.618 ± 0.18	13.55 ± 0.7	1.600 ± 0.19	–		–		−0.56 ± 0.3	0.059 ± 0.03
3 ↔ 1 TTA	–		–		–		10.76 ± 0.5	2.25 ± 0.26	16.13 ± 0.7	3.63 ± 0.40	–	
3 ↔ 1 xl-TTA	–		4.89 ± 0.4	0.957 ± 0.15	4.87 ± 0.5	0.916 ± 0.16	5.63 ± 0.4	1.12 ± 0.14	12.02 ± 0.6	2.54 ± 0.33	−11.9 ± 0.2	2.11 ± 0.17

one-step hypothetical triplex-to-coil transition using a simple additive approach, as described and discussed below.

Crosslinking Increases the Number of Protons Released upon Triplex Melting. The hairpin duplex portion of the intramolecular triple helix is unprotonated at all pH values above pH 6.0. Consequently, a comparison of the degree of proton release (Δk) accompanying denaturation of the uncrosslinked and crosslinked triplex structures at pH 7.0 should not be affected by the crosslinking-induced change in the path of the transition from 3 ↔ 2 ↔ 1 to 3 ↔ 1. Inspection of the Δk data in the final column of Table 2 reveals, that melting of the crosslinked triplex to its coil state results in a release of fractionally more protons ($\Delta k = 2.11$) than the corresponding melting of the uncrosslinked triplex (i.e., $\Delta k = 1.71$), such that $\Delta\Delta k = 0.4$. Since our disulfide crosslink should not result in a change in the number of protonatable sites in the pH range between pH 4.0 and pH 8.0, this increase in Δk requires a more subtle explanation. In developing such an explanation, it should be noted that the enhanced proton release we observe upon melting of the crosslinked structure occurs at pH values considerably more than one pH unit removed from the pK_a of any of the free bases (Saenger, 1984). Consequently, in the absence of some unusual pK_a shift induced by the lariat coil structure, it is unlikely that the denatured states of either the crosslinked or the uncrosslinked structure remain protonated at these pH values. Thus, the difference we observe in the degree of proton release should reflect differences in the degree of protonation of the initial triplex states. In focusing on these triplex states, it is interesting to note that the calculated number of protons released for either third strand bears no direct relation to the number of cytosines in the third strand that can be protonated, an observation consistent with a previous study on another intramolecular triplex (Plum & Breslauer, 1995). Furthermore, it has been found that, when separated by intervening thymidines, all third-strand cytosines are protonated to a similar degree (Völker & Klump, 1994; Hüsler & Klump, 1995; Plum & Breslauer, 1995). In light of these observations, we propose that the difference observed between the number of protonatable sites and the actual number of protons released upon triplex melting at pH 7.0 is consistent with a rapid equilibrium between free protons and triplex-bound protons. Thus, the apparent increase in the number of protons released from the crosslinked structure may simply reflect a crosslinking induced change in the equilibrium between the bound and unbound protons (i.e., a change in apparent pK_a). This potential explanation is reasonable since binding to double-stranded DNA has been shown to cause shifts in the apparent pK_a of various drugs (Lamm & Pack, 1990; Misra & Honig, 1994; Jones & Wilson, 1981) and of Hoogsteen third-strand cytosine residues (Völker et al., 1993; Plum & Breslauer, 1995; Sklenar & Feigon, 1990; Singleton & Dervan, 1992), so it is not surprising that the crosslink investigated here could cause a similar effect. We therefore propose that the further increase in the apparent pK_a of the crosslinked structure relative to its uncrosslinked parent observed in this work is due to the chemical constraint of the crosslink which keeps the Hoogsteen strand in proximity with the major groove. This point of view is supported by NMR studies on the crosslinked structure (Osborne et al., 1996b) which show that the observed increase in the apparent pK_a of the third-strand cytosines depends on the length of the link used

to crosslink the third strand to the major groove of the triple helix. An alternative explanation, which cannot be ruled out based on the results presented here, envisions only some, rather than all, of the third-strand cytosines being protonated within a given molecule. In this case, the observed increase in the number of protons released from the crosslinked molecule would be due to a larger fraction of protonated cytosines in the crosslinked triple helical structure.

Crosslinking Reduces the Number of Counterions Released upon Triplex Melting. Inspection of the Δn data listed in Table 2 allows one to compare the calculated degree of counterion release for the hypothetical $3 \leftrightarrow 1$ transition of the uncrosslinked oligonucleotide ($\Delta n = 2.24$) with the observed $3 \leftrightarrow 1$ transition of the crosslinked oligonucleotide at pH 7.0 ($\Delta n = 0.96$). This comparison reveals a significant $\Delta\Delta n$ difference of ≈ -1.3 Na^+. Since counterions are condensed onto both the native and denatured states of the molecules, the calculated degree of counterion release for each conformational transition only reflects the net difference in the number of counterions associated with the initial and final states. Consequently, the difference we observe in the number of counterions released for the crosslinked and uncrosslinked structures ($\Delta\Delta n = 1.3$ Na^+) reflects crosslinking-induced differences in the interaction of the counterions with the native and denatured states. Some of this difference should be due to the disparity in the number of protons associated with the native triplex states of the crosslinked and uncrosslinked structures (*vide supra*). Assuming that protons substitute for Na^+ counterions on a *one-to-one* basis (i.e., neglecting nonideality due to site-binding and "cross-talk") (Record et al., 1976), we can simply subtract the differences in the number of protons released ($\Delta\Delta k = 0.4$) as determined above, from the difference in the degree of Na^+ counterion release ($\Delta\Delta n = 1.3$), to obtain an overall difference of 0.9 "counterions". In view of the total number of Na^+ counterions and protons released from the triplex, we believe that this difference is too large to originate entirely from the nonideal behavior of protons. Hence, it seems likely that fewer counterions are released when the crosslinked molecule denatures to the coil state, a circumstance consistent with the reduced entropic driving force for melting of the crosslinked triplex. This observation is in agreement with melting studies on DNA dumbbells which also produce constrained final states, but which have initial states that are not complicated by protonation (Erie et al., 1989).

CONCLUSIONS

We have shown that constraining an intramolecular triplex via disulfide bridges induces profound changes in triplex properties. Specifically, we found crosslinking induces a large increase in triplex thermal stability and alters the triplex melting pathway by obliterating the intermediate duplex state formed during melting of the unconstrained triplex. From temperature- and pH dependent optical melting data, we have constructed phase diagrams for the uncrosslinked and crosslinked triplexes. These diagrams define the state that exists in solution at a given set of pH and temperature values, while also allowing one to predict the transition(s) that will be induced by a given change in temperature and/or pH. Calorimetric melting studies allowed us to characterize thermodynamically the consequences of crosslinking. We found that crosslinking induces an increase in triplex stability of nearly 3 kcal/mol, with this stabilization being entirely due to a decrease in the entropic driving force favoring melting of the crosslinked structure. In other words, the impact of crosslinking is enthalpically neutral. We also have shown that crosslinking increases the number of protons and reduces the number of counterions that are released upon triplex melting. In the aggregate, our results reveal and characterize the profound impact that crosslinking can have on triplex stability and melting behavior. Such assessments are important in a range of practical applications where one must rationally modulate triplex properties. On a more fundamental level, our results contribute to the characterization of the molecular forces that stabilize/destabilize Watson−Crick and non-Watson−Crick nucleic acid structures.

ACKNOWLEDGMENT

Jens Völker thanks Drs. Tigran V. Chalikian, G. Eric Plum, and Nataša Poklar for many stimulating discussions and helpful suggestions during the course of this work.

REFERENCES

Amaratunga, M., Snowden-Ifft, E., Wemmer, D. E., & Benight, A. S. (1992) *Biopolymers 32*, 865−879.
Ashley, G. W., & Kushlan D. M. (1991) *Biochemistry* 30, 2927−2933.
Baldwin, R. L. (1971) *Acc. Chem. Res. 4*, 265−272.
Benight A. S., Schurr, J. M., Flynn, P. F., Reid, B. R., & Wemmer, D. E. (1988) *J. Mol. Biol. 200*, 377−399.
Breslauer, K. J. (1986) in *Thermodynamic Data for Biochemistry and Biotechnology* (Hinz, H. J., Ed.), pp 402−427, Springer Verlag, New York.
Breslauer, K. J. (1994) in *Methods in Molecular Biology, Vol 26: Protocols for Oligonucleotide Conjugates* (Agrawal, S., Ed.) Chapter 14, pp 347−372, Humana Press, Inc., Totowa, NJ.
Breslauer, K. J. (1995) *Methods Enzymol. 259*, 221−242.
Breslauer, K. J., Frank, R., Blöcker, H., & Marky, L. A. (1986) *Proc. Natl. Acad. Sci. U.S.A. 83*, 3746−3750.
Cain, H., Zuiderweg, E. R. P., & Glick, G. D. (1995) *Nucleic Acids Res. 23*, 2153−2160.
Callahan, D. E., Trapane, T. L., Miller, P. S., Ts'o, P. O. P., & Kan, L-S. (1991) *Biochemistry 30*, 1650−1655.
Cantor, C. R., Warshaw, M. M., & Shapiro, H. (1970) *Biopolymers 9*, 1059−1077.
Cantor, C. R., & Schimmel, P. R. (1980a) *Biophysical Chemistry, Part II: Techniques for the Study of Biological Structure and Function*, W. H. Freeman & Company, San Franscisco.
Cantor, C. R., & Schimmel, P. R. (1980b) *Biophysical Chemistry Part III: The Behaviour of Biological Macromolecules*, W. H. Freeman & Company: San Franscisco.
Cheng, Y.-K., & Pettitt, B. M. (1992) *Prog. Biophys. Mol. Biol. 58*, 225−257.
Craig, M. E., Crothers, D. M., & Doty, P. (1971) *J. Mol. Biol. 62*, 383−401.
Doktycz, M. J., Goldstein R. F., Paner, T. M., Gallo F. J., & Benight, A. S. (1992) *Biopolymers 32*, 849−864.
Doktycz, M. J., Paner, T. M., & Benight, A. S. (1993) *Biopolymers 33*, 1765−1777.
Durand, M., Peloille, S., Thuong, N. T., & Maurizot, J. C. (1992) *Biochemistry 31*, 9197−9204.
Elson, E. L., Scheffler, I. E., & Baldwin, R. L. (1970) *J. Mol. Biol. 54*, 401−415.
Erie, D. A., Jones, R. A., Olson, W. K., Sinha, N. K., & Breslauer, K. J. (1987) *Biochemistry 26*, 7150−7159.
Erie, D. A., Sinha, N. K., Olson, W. K., Jones, R. A., & Breslauer, K. J. (1989) *Biochemistry 28*, 268−273.
Ferentz, A. E., & Verdine, G. L. (1991) *J. Am. Chem. Soc. 113*, 4000−4002.
Ferentz, A. E., Keating, T. A., & Verdine, G. L. (1993) *J. Am. Chem. Soc. 115*, 9006−9014.
Germann, M. W., Schoenwaelder, K.-H., & van de Sande, J. H. (1985) *Biochemistry 24*, 5698−5702.
Glick, G. D. (1991) *J. Org. Chem. 56*, 6746−6747.

Glick, G. D., Osborne, S. E., Knitt, D. S., & Marino, J. P., Jr. (1992) *J. Am. Chem. Soc. 114*, 5447−5448.
Goodwin, J. T., & Glick, G. D. (1993) *Tetrahedron Lett. 34*, 5549−5552.
Goodwin, J. T., Osborne, S. E., Swanson, P. C., & Glick, G. D. (1994) *Tetrahedron Letters 35*, 4527−4530.
Gray, D. M., Hung, S.-H., & Johnson, K. H. (1995) *Methods Enzymol. 246*, 19−34.
Häner, R., & Dervan, P. B. (1990) *Biochemistry 29*, 9761−9765.
Hoogsteen, K. (1959) *Acta Crystallogr. 12*, 822−823.
Hüsler, P. L., & Klump, H. H. (1995) *Arch. Biochem. Biophys. 317*, 46−56.
Jacobson, H., & Stockmeyer, W. H. (1950) *J. Chem. Phys. 18*, 1600−1606.
Jones, R. L., & Wilson, W. D. (1981) *Biopolymers 20*, 141−154.
Kool, E. T. (1991) *J. Am. Chem. Soc. 113*, 6265−6266.
Kool, E. T. (1996) *Annu. Rev. Biophys. Biomol. Struct. 25*, 1−28.
Lamm, G., & Pack, G. R. (1990) *Proc. Natl. Acad. Sci. U.S.A. 87*, 9033−9036.
Macaya, R. F., Gilbert, D. E., Malek, S., Sinsheimer, J. S., & Feigon, J. (1991) *Science 254*, 270−274.
MacGregor, Jr., R. B. (1996) *Biopolymers 38*, 321−327.
Manning, G. S. (1978) *Q. Rev. Biophys. 11*, 179−246.
Marky, L. A., & Breslauer, K. J. (1987) *Biopolymers 26*, 1601−1620.
Misra, V. K., Sharp, K. A., Friedman, R. A., & Honig, B. (1994) *J. Mol. Biol. 238*, 245−263.
Olmsted, M. C., Anderson, C. F., & Record, T. M., Jr. (1989) *Proc. Natl. Acad. Sci. U.S.A. 86*, 7766−7770.
Olmsted, M. C, Anderson, C. F., & Record, M. T., Jr. (1991) *Biopolymers 31*, 1593−1604.
Osborne, S. E., Völker, J., Stevens, S. Y., Breslauer, K. J., & Glick, G. D (1996a) *J. Am. Chem. Soc. 118*, 11993−12003.
Osborne, S. E., Cain, R. J., & Glick, G. D. (1996b) *J. Am. Chem. Soc.* (in press).
Paner, T. M., Amaratunga, M., & Benight, A. S. (1992) *Biopolymers 32*, 881−892.
Pfeil, W., & Privalov, P. L. (1976) *Biophys. Chem. 4*, 23−32.
Pilch, D. S., Plum, G. E., & Breslauer, K. J. (1995) *Curr. Opin. Struct. Biol. 5*, 334−342.
Plum, G. E., Park, Y-W., Singleton, S. F., Dervan, P. B., & Breslauer, K. J. (1990) *Proc. Natl. Acad. Sci. U.S.A. 87*, 9436−9440.
Plum, G. E., Pilch, D. S., Singleton, S. F., & Breslauer, K. J. (1995) *Annu. Rev. Biophys. Biomol. Struct. 24*, 319−350.
Plum, G. E., & Breslauer, K. J. (1995) *J. Mol. Biol. 248*, 679−695.
Pörschke, D. (1971) *Biopolymers 10*, 1989−2013.
Pörschke, D. (1977) *Mol. Biol. Biochem. Biophys. 24*, 191−218.
Pörschke, D., & Eigen, M. (1971) *J. Mol. Biol. 62*, 361−381.
Prakash, G., & Kool, E. T. (1991) *J. Chem. Soc., Chem. Commun.* No. 17, 1161−1163.
Prakash, G., & Kool, E. T. (1992) *J. Am. Chem. Soc. 114*, 3523−3527.
Ptitsyn, O. B., & Birshtein, T. M. (1969) *Biopolymers 7*, 435−445.
Radhakrishnan, I., & Patel, D. J. (1993) *J. Am. Chem. Soc. 115*, 1615−1617.
Radhakrishnan, I., & Patel, D. J. (1994a) *J. Mol. Biol. 241*, 600−619.
Radhakrishnan, I., & Patel, D. J. (1994b) *Structure 2*, 17−32.
Radhakrishnan, I., & Patel, D. J. (1994c) *Biochemistry 33*, 11405−11416.
Radhakrishnan, I., Gao, X., de los Santos, C., Live, D., & Patel, D. J. (1991a) *Biochemistry 30*, 9022−9030.
Radhakrishnan, I., Patel, D. J., & Gao, X. (1991b) *J. Am. Chem. Soc. 113*, 8542−8544.
Radhakrishnan, I., Patel, D. J., & Gao, X. (1992a) *Biochemistry 31*, 2514−2523.
Radhakrishnan, I., Patel, D. J., Veal, J. M., & Gao, X. (1992b) *J. Am. Chem. Soc. 114*, 6913−6915.
Radhakrishnan, I., de los Santos, C., & Patel, D. J. (1993a) *J. Mol. Biol. 234*, 188−197.
Radhakrishnan, I., Patel, D. J., Priestley, E. S., Nash, H. M., & Dervan, P. B. (1993b) *Biochemistry 32*, 11228−11234.
Rentzeperis, D., & Marky, L. A. (1995) *J. Am. Chem. Soc. 117*, 5423−5424.
Record, M. T., Jr., & Lohman, T. M. (1978) *Biopolymers 17*, 159−166.
Record, M. T., Jr., Woodbury, C. P., & Lohman, T. M. (1976) *Biopolymers. 15*, 893−915.
Record, M. T., Jr., Anderson, C. F., & Lohman, T. M. (1978) *Q. Rev. Biophys. 11*, 103−178.
Robinson, R. A., & Stokes, R. H. (1959) *Electrolyte Solutions*, 2nd ed., Academic Press, New York.
Rubin, E., & Kool, E. T. (1994) *Angew. Chem., Int. Ed. Engl. 33*, 1004−1007.
Rumney, S., IV, & Kool, E. T. (1992) *Angew. Chem., Int. Ed. Engl. 31*, 1617−1619.
Saenger, W. (1983) *Principles of Nucleic Acid Structure*, Springer-Verlag, Berlin.
SantaLucia, J., Jr., Allawi, H. T., & Seneviratne, P. A. (1996) *Biochemistry 35*, 3555−3562.
Scheffler, I. E., Elson, E. L., & Baldwin, R. L. (1970) *J. Mol. Biol. 48*, 145−171.
Seeman, N. C., & Kallenbach, N. R. (1994) *Annu. Rev. Biophys. Biomol. Struct. 23*, 53−86.
Sklenar, V., & Feigon, J. (1990) *Nature 345*, 836−838.
Singleton, S. F., & Dervan, P. B. (1992) *Biochemistry 31*, 10995−11003.
Snell, F. D., & Snell, C. T. (1949) *Colorimetric Methods of Analysis*, 3rd ed., Vol. 2, p 671, Van Nostrand, New York.
Soyer, V. N., & Potaman, V. N. (1995) *Triple Helical Nucleic Acids*, Springer-Verlag, New York.
Steely, H. T., Gray, D. M., & Ratliff, R. L. (1986) *Nucleic Acids Res. 14*, 10071−10090.
Sun, J.-S., & Helene, C. (1993) *Curr. Opin. Struct. Biol. 3*, 345−356.
Thuong, N. T., & Helene, C. (1993) *Angw. Chem., Int. Ed. Engl. 32*, 666−690.
van de Sande, J. H., Ramsig, N. B., Germann, M. W., Elhorst, W., Kalisch, B. W., v. Kitzing, E., Pon, R. T., Clegg, R. C., & Jovin, T. M. (1988) *Science 241*, 551−557.
Vo, T., Wang, S., & Kool, E. T. (1995) *Nucleic Acids Res. 23*, 2937−2944.
Völker, J., & Klump, H. H. (1994) *Biochemistry 33*, 13502−13508.
Völker, J., Botes, D. P., Lindsey, G. G., & Klump, H. H. (1993) *J. Mol. Biol. 230*, 1278−1290.
Wang, E., Malek, S., & Feigon, J. (1992) *Biochemistry 31*, 4838−4846.
Wang, H., Osborne S. E., Zuiderweg, E. R. P., & Glick, G. D. (1994) *J. Am. Chem. Soc. 116*, 5021−5022.
Wang, H., Zuiderweg, E. R. P, & Glick G. D. (1995) *J. Am. Chem. Soc. 117*, 2981−2991.
Weast, R. C., Ed. (1982) *CRC Handbook of Chemistry and Physics*, 63rd ed., pp D-261−262, CRC Press, Inc., Boca Raton, FL.
Wemmer, D. E., & Benight, A. S. (1985) *Nucleic Acids Res. 13*, 8611−8621.
Williamson, J. R. (1994) *Annu. Rev. Biophys. Biomol. Struct. 23*, 703−730.
Wilson, W. D., Hopkins, H. P., Mizan, S., Hamilton, D. D., & Zon, G. (1994) *J. Am. Chem. Soc. 116*, 3607−3608.

BI962271L